

# UC Riverside

## UC Riverside Previously Published Works

### Title

Structure-Based Design of Novel EphA2 Agonistic Agents with Nanomolar Affinity in Vitro and in Cell

### Permalink

<https://escholarship.org/uc/item/2887v3dx>

### Journal

ACS Chemical Biology, 13(9)

### ISSN

1554-8929

### Authors

Gambini, Luca  
Salem, Ahmed F  
Udompholkul, Parima  
[et al.](#)

### Publication Date

2018-09-21

### DOI

10.1021/acscchembio.8b00556

Peer reviewed



# HHS Public Access

Author manuscript

ACS Chem Biol. Author manuscript; available in PMC 2019 June 27.

Published in final edited form as:

ACS Chem Biol. 2018 September 21; 13(9): 2633–2644. doi:10.1021/acscchembio.8b00556.

## Structure-Based Design of Novel EphA2 Agonistic Agents with Nanomolar Affinity *in Vitro* and in Cell

Luca Gambini<sup>†</sup>, Ahmed F. Salem<sup>†</sup>, Parima Udompholkul<sup>†</sup>, Xiao-Feng Tan<sup>‡</sup>, Carlo Baggio<sup>†</sup>, Neh Shah<sup>†</sup>, Alexander Aronson<sup>†</sup>, Jikui Song<sup>‡</sup>, and Maurizio Pellecchia<sup>\*,†</sup>

<sup>†</sup> Division of Biomedical Sciences, School of Medicine, University of California Riverside, 900 University Avenue, Riverside, California 92521, United States

<sup>‡</sup> Department of Biochemistry, College of Natural and Agricultural Sciences, University of California Riverside, 900 University Avenue, Riverside, California 92521, United States

### Abstract

EphA2 overexpression is invariably associated with poor prognosis and development of aggressive metastatic cancers in pancreatic, prostate, lung, ovarian, and breast cancers and melanoma. Recent efforts from our laboratories identified a number of agonistic peptides targeting the ligand-binding domain of the EphA2 receptor. The individual agents, however, were still relatively weak in affinities (micromolar range) that precluded detailed structural studies on the mode of action. Using a systematic optimization of the 12-mer peptide mimetic 123B9, we were able to first derive an agent that displayed a submicromolar affinity for the receptor. This agent enabled cocrystallization with the EphA2 ligand-binding domain providing for the first time the structural basis for their agonistic mechanism of action. In addition, the atomic coordinates of the complex enabled rapid iterations of structure-based optimizations that resulted in a novel agonistic agent,

\*Corresponding Author Tel.: (951) 827-7829. maurizio.pellecchia@ucr.edu.

#### Author Contributions

L.G. and A.F.S. contributed equally to this work. M.P. designed the research strategy for the novel peptides, including the selection of novel P1 derivatives and cyclic agents as described in Tables 1 and 2. M.P. directed research by L.G., A.F.S., C.B., P.U., N.S., A.A., and coordinated structural studies with J.S. and his associate X.-F.T. L.G. synthesized, purified, and characterized most of the agents reported in Tables 1 and 2, performed ITC measurements, and proposed inserting the FRP region into 123B9 and derivatives. A.F.S. devised methods to characterize the agents in all of the reported cellular assays and carried out these studies. P.U. conducted biochemical assays for all compounds listed in Tables 1 and 2. C.B. provided purified protein that was used for all *in vitro* assays and structural studies and performed some of the ITC measurements and the NMR measurements of Figure S6. N.S. assisted A.F.S. in carrying out several of the cell based assays. A.A. helped L.G. in preparing some reagents and peptides. X.-T.F., under the supervision of J.S., obtained the X-ray structure of the complex and prepared Table S1. M.P. with A.F.S. and L.G., and some help from other authors, wrote the manuscript. L.G., with the help of A.F.S. and P.U., prepared Figures 1, 3, S1, S2, S4, and S5 and Table S2. A.F.S. prepared Figures 4, 5, and S3. M.P. prepared all structural figures (except for Figure 1, S4, and S5), and analyzed with the various authors all data reported in the manuscript.

#### ASSOCIATED CONTENT

##### Supporting Information

The Supporting Information is available free of charge on the ACS Publications website at DOI: [10.1021/acscchem-bio.8b00556](https://doi.org/10.1021/acscchem-bio.8b00556). Crystallographic parameters (Table S1), mass spectroscopy data of investigated compounds (Table S2), the synthetic scheme used to prepare dimeric agents (Figure S1), ITC curves for compounds 135G10 and 135I4 against EphA2 (Figure S2), additional data relative to time lapse migration assay of BxPC3 cells (Figure S3), a schematic illustration of the interactions between 135E2 and EphA2-LBD (Figure S4), a schematic illustration of the interactions between 135H11 and EphA2-LBD (Figure S5), 1D <sup>1</sup>H NMR and 2D [<sup>15</sup>N, <sup>1</sup>H] so-fast HSQC NMR spectra of <sup>15</sup>N-EphA2-LBD measured in absence and in the presence of various concentrations of 135H11 (Figure S6) (PDF)

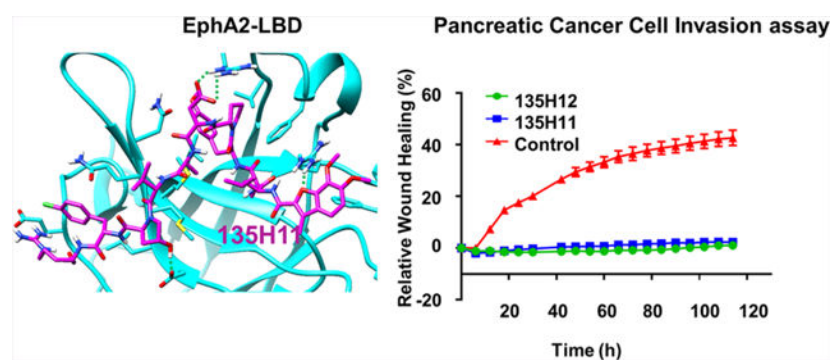
##### Accession Codes

PDB ID 6B9L

The authors declare no competing financial interest.

named 135H11, with a nanomolar affinity for the receptor, as demonstrated by *in vitro* binding assays (isothermal titration calorimetry measurements), and a biochemical displacement assay. As we have recently demonstrated, the cellular activity of these agents is further increased by synthesizing dimeric versions of the compounds. Hence, we report that a dimeric version of 135H11 is extremely effective at low nanomolar concentrations to induce cellular receptor activation, internalization, and inhibition of cell migration in a pancreatic cancer cell line. Given the pivotal role of EphA2 in tumor growth, angiogenesis, drug resistance, and metastasis, these agents, and the associated structural studies, provide significant advancements in the field for the development of novel EphA2-targeting therapeutics or diagnostics.

## Graphical Abstract



EphA2 belongs to a class of receptor tyrosine kinases that have been implicated in tumorigenesis, drug resistance, and metastatic behaviors of several solid tumors including prostate cancer;<sup>1-3</sup> melanoma;<sup>4</sup> urinary bladder,<sup>5</sup> breast,<sup>6</sup> ovarian,<sup>7</sup> pancreatic,<sup>8-10</sup> brain,<sup>11-13</sup> esophagus,<sup>14</sup> lung,<sup>15</sup> and stomach<sup>16</sup> cancers; and leukemia.<sup>17-20</sup> In cancer cells, the unbalanced overexpression of the receptor compared to its ligands (*ephrin-A*) primes the EphA2 pro-oncogenic activity. Hence, unligated EphA2 receptor functions as an oncogene, and its effect can be reverted by stimulation by agonistic agents, which, once engaged with the receptor, stimulate intrinsic tumor suppressive signaling pathways mediated by the EphA2.<sup>21</sup> Structurally, EphA2 is composed of an extracellular domain, responsible for engagement with the *ephrin-A* ligands. *Ephrin-A* ligand binding causes receptor dimerization, clustering, and internalizations. The cytosolic region of the receptor contains a kinase domain, a SAM domain, and a PDZ binding motif that trigger the cellular signaling events. Because of its possible dual role as an oncogene and a tumor suppressor, EphA2 is currently the subject of fervid research for the development of possible therapeutics that target either its intracellular kinase domain<sup>22-25</sup> or its ligand binding domain.<sup>26,27</sup> Because receptor activation reverts the prooncogenic function of the EphA2, small molecule EphA2 agonists hold great potential for the development of novel therapeutics. Recently, antibodies directed at the ligand-binding domain were shown to have the ability to suppress tumor growth in human breast cancer (MDA-MB-231) and in human gastric cancer (SNU-16) xenograft mouse models.<sup>27</sup> More recently, we have developed novel EphA2 dimeric agonist peptides conjugated with the chemotherapeutic agent paclitaxel and demonstrated that dimerization of the peptides can trigger receptor activation at lower concentrations (compared to the monomeric peptides) and that the activated EphA2-peptide complex

internalized its cargo, hence, effectively working as a molecular Trojan horse for EphA2 expressing cancer cells.<sup>28</sup> However, the carrying agonistic peptides remained of relatively weak affinity, limiting the full potential of these agents as effective EphA2 therapeutics. Indeed, potent agonistic agents could be conjugated with either chemotherapy, for use as peptide–drug conjugates (PDCs), or with fluorophores, metal-chelating groups for PET or MRI, for use as diagnostics. In our previous studies, we used a 12-mer agonistic peptide with a relatively weak affinity for EphA2 to derive PDCs and exploited peptide dimerization to bootstrap cellular activity from triple-digit micromolar to low micromolar. In the current study, we first deployed more extensive structure–activity relationship studies to obtain an EphA2 agonistic agent with low micromolar affinity. This allowed us to obtain a crystal structure of the complex between such an agent and the EphA2 ligand-binding domain. Hence, using structure-based approaches, we were able to derive novel and more potent EphA2 binding agents that displayed nanomolar affinity for the receptor as determined by isothermal titration calorimetry and *in vitro* displacement assays. A dimeric version of the most potent agent was extraordinarily effective in cellular assays for receptor degradation, and suppression of pro-oncogenic activity of EphA2 in cellular models, including a remarkable inhibition of both pancreatic cancer cell migration and invasion.

## RESULTS

### Initial Optimization of 123B9 Based on Primary Sequences of *ephrin* Ligands.

In order to more rapidly and accurately characterize the binding properties of novel 123B9 (Table 1) derived EphA2-binding agents, we first developed a DELFIA assay (Figure 1A). Briefly, a biotinylated 123B9 peptide was prepared and used as bait in streptavidin-coated 96-well plates (PerkinElmer). Subsequently, the 6XHis-EphA2-ligand-binding domain (LBD) was added to each assay well, together with a highly fluorescent Europium-conjugated anti-6XHis antibody. Hence, after incubation with a test agent and washing steps, residual fluorescence indirectly measured the ability of the given test compound to displace 123B9 from EphA2. In repeated experiments, the  $Z'$  factor of this assay was 0.76, indicating that the approach was very robust as a primary assay to conduct the proposed studies. In this assay, the previously reported peptides YSA (YSAYPDSVPMMS)<sup>29</sup> and 123B9<sup>30</sup> (Table 1) displayed  $IC_{50}$  values of 16.5  $\mu M$  and 6.5  $\mu M$ , respectively, again in close agreement with our previous isothermal titration calorimetry studies with these agents (Table 1, Figure 1B).<sup>30</sup>

A number of putative peptide-binding regions derived from known protein binders to EphA2 (the *ephrin-A* ligands and an EphA2 antibody, named 1C1; Figure 1C) were identified, synthesized, and tested, given their resemblances to 123B9 and YSA (Table 1). However, none of these peptides displayed increased affinity for the EphA2-LBD compared to 123B9 (Table 1). Subsequently, we derived several “chimeric” peptides iteratively inserting elements of active peptides into these *ephrin* derived peptides. To expedite the synthesis, we first kept a Tyr at the N-terminus, and subsequently, we reintroduced the Tyr isostere present in 123B9 (namely, 4F,3Cl phenyl acetic acid; Table 1) that we had incorporated into EphA2 targeting peptides to increase their plasma stability.<sup>30</sup> These initial studies revealed unexpectedly that introducing the C-terminal region of the *ephrin* ligands (sequence FRP)

into 123B9 resulted in agent 135E2 (and the corresponding N1-Tyr equivalent, 135B12) that was significantly more potent than the initial agents (Table 1). Subsequently, a second round of optimizations focused on modifications of the C-terminal peptide region and the introduction of non-natural amino acids in the attempt to further increase affinity for the receptor. These studies culminated in agent 135G3 that displayed an IC<sub>50</sub> value of 600 nM in the DELFIA assay (Table 1, Figure 1B). To further validate the DELFIA displacement assay values and the selectivity of the resulting agent, we performed isothermal titration calorimetry measurements for selected agents against the ligand-binding domains of EphA2 and EphA4 (Figure 1D). These data revealed that 135G3 bound to the EphA2-LBD with a dissociation constant of 757 nM, hence comparable to the DELFIA IC<sub>50</sub> value. In addition, no significant binding was detected against the EphA4, confirming that the resulting agent had preserved its selectivity (Figure 1D).

Agonistic agents, such as the ephrin ligands, cause receptor dimerization that cause phosphorylation of the kinase domain. Hence, to assess the agonistic activity of our compounds in the cell, we could directly measure the phosphorylation levels of the EphA2 as illustrated in Figure 1E. In this cellular assay, 135G3 resulted more effective in inducing receptor phosphorylation compared to both YSA and 135B12, which is in agreement with relative *in vitro* binding affinities of these agents to the receptor (Figure 1E).

### The X-ray Structure of 135E2 in Complex with the EphA2 Ligand-Binding Domain.

Crystallization conditions were tested through sparse-matrix screening (Hampton Research Inc.) for 135E2 in complex with the ligand binding domain of the EphA2. The crystals were subsequently reproduced using the hanging-drop vapor diffusion method at 4 °C, from drops mixed with 1  $\mu$ L of protein complex and 1  $\mu$ L of precipitant solution (0.1 M Tris-Cl, pH 8.0, 1.4–1.8 M Li<sub>2</sub>SO<sub>4</sub>). Crystals were soaked for a few seconds in a cryoprotectant solution, composed of crystallization solution and 20% glycerol, before flash freezing in liquid nitrogen. Data were subsequently collected at the 5.0.1 beamline at the Advanced Light Source, Lawrence Berkeley National Laboratory, and the diffraction data were indexed, integrated, and scaled using the HKL2000 program.<sup>31</sup> The structure was finally solved using the molecular replacement method in PHASER,<sup>32</sup> using the PDB ID code 3C8X as a search model. The structure of the complex was refined by iterative model building using Coot<sup>33</sup> and PHENIX software packages.<sup>34</sup> The statistics for data collection and structural refinement of the EphA2–peptide complex are summarized in Supporting Information Table S1. The structure of 135E2 in complex with the EphA2-LBD is reported in Figure 2A together with structural superposition with the loop region from ephrinA5 bound to EphA2 (PDB ID 3MX0; Figure 2B). While there is a good structural agreement in the positioning of the peptide and ephrinA5 loop region within the N-terminus region, the peptide departs for the ephrinA5 bound conformation to form a more extended structure. Hence, the gain in activity obtained by the introduction of the C-terminal FRP sequence from the ephrin ligands into 123B9 was serendipitous. In this regard, in addition to intermolecular interactions involving residue 135E2 Asp6 with EphA2 Arg159, we also observed an additional salt bridge between 135E2 Arg11 with EphA2 Glu40 that supported the observed increased activity of the agents compared to YSA and 123B9 (Figure 2A,C). Finally, the presence of a hydrogen bond between Arg103 and the ether oxygen on the 4F,3Cl phenyl

acetic acid moiety supported the observed increased activity of 123B9 versus YSA (Figure 2A, Table 1).

### Structure-Based Optimization of 135E2.

Using structure-based design strategies and the structure of the complex between 135E2 and EphA2-LBD, we have subsequently designed novel agents with improved affinity over 135G3. Given the bent bound conformation that juxtaposes the two serine residues in 135E2 (Figure 2A,C, Supporting Information Figure S4), we first sought to stabilize this intramolecular interaction either covalently or noncovalently (Table 2, agents 135G8, 135G9, 135F11, 135G10, 135I2, and 135I3). Cyclization of the compound using two Cys and a disulfide bridge (135G8) or introducing a Glu-Dap (diamino-propionic acid) lactam (135G9) resulted in less potent agents (Table 2). However, replacement of a disulfide bond between a Cys in position 2 and a homo-Cys in lieu of Ser 5 (but not the contrary arrangement, as in 135I2) resulted in cyclic agent 135I3 with retained affinity ( $IC_{50} \sim 1 \mu M$ ; Table 2). Introducing a possible intramolecular salt bridge, hence replacing Ser2 and Ser5 with Dap and Asp, respectively, resulted in agent 135F11 that displayed a marked loss in affinity for EphA2. However, stabilizing the bound conformation with two hydrophobic residues in lieu of Ser2 and Ser5 (namely, Leu2 and Ala5) resulted in an agent with a significantly increased affinity (135G10,  $IC_{50} = 0.22 \mu M$ , Table 2). ITC measurements with 135G10 confirmed that the increased affinity was driven by a reduced loss in entropy upon binding compared to the parent agent 135G3 (135G3  $H = -21.9$  kcal/mol,  $-T \Delta S = 13.5$  kcal/mol, Figure 1; 135G10,  $H = -19.4$  kcal/mol,  $-T \Delta S = 10.6$  kcal/mol, Supporting Information Figure S2), although the enthalpy/entropy compensation phenomena significantly damped the potential gain in affinity.<sup>35,36</sup>

Further introduction of non-natural amino acids (agents 135G11 to 135H4) at various positions resulted in agent 135G11, with slightly improved  $IC_{50}$  value (Table 2).

Next, we examined the binding pose for the 4F,3Cl phenyl-acetic acid moiety of 135E2 and designed novel restrained analogues. Molecular modeling studies based on the structure 135E2 in complex with EphA2 were conducted, and these efforts resulted in the design and synthesis of a series of substituted benzofuranoic acids (agents 135G6 to 135H11, Table 2). These studies culminated with the selection of a 3-methyl, 6,7-dimethoxy, 2-benzofuranoic acid in 135E2 that resulted first in 135G6 and later in 135H11 (including all optimizing features), a novel agent with increased affinity for EphA2 (Figure 3, Table 2, Supporting Information Figure S5). Modeling studies anticipated the formation of additional intermolecular hydrogen bonding between the 3-methyl, 6,7dimethoxy, 2-benzofuranoic acid moiety and Arg 103 in EphA2 (Figure 3B). Finally, the Tyr residues in the fourth position seemed engaged in a fairly hydrophobic area of the binding pocket; hence it was replaced by a 4-methoxy Phe. 135H11 displayed increased affinity by ITC compared to other agents (Figure 3C) and retained selectivity when tested against the EphA4 (Figure 3D). Its constrained cyclic equivalent (135I4, Table 2) presented a similar  $IC_{50}$  value in the DELFIA assay, and its binding affinity was driven by a reduced loss in entropy upon ligand binding (Supporting Information Figure S2). However, this entropic gain was entirely compensated by a dramatic loss in enthalpy of binding, suggesting a nonideal geometry of

the constrained peptide to interact with the ligand-binding domain of EphA2 (Supporting Information Figure S2). These data concluded that the cyclic agent 135I4 is potentially a novel and interesting agent that could be subjected to optimization of its side chains to increase its enthalpy of binding, in addition to replacement of the disulfide bridge with more stable moieties.

Therefore, collectively, these data suggested that linear agents 135G3 and 135H11 were the most suitable candidates for further studies at this stage of our hit-to-lead optimizations. Additional binding assays involved the use of 1D  $^1\text{H}$  NMR and 2D [ $^{15}\text{N}$ ,  $^1\text{H}$ ] correlation spectra with a  $^{15}\text{N}$  labeled sample of EphA4-LBD. The spectra were collected in the absence and in the presence of various amounts of 135H11. The data are reported in Supporting Information Figure S6. Upon titration of 135H11, EphA4 resonances progressively disappeared, while new cross-peaks appeared, typical of binders in slow-exchange on the NMR time scale (Supporting Information Figure S6). While it is not possible to measure the dissociation constant by NMR titration in slow exchange, measuring the chemical shift differences of cross-peaks in the free versus bound form, we estimated an upper limit for the off rate for the complex,  $k_{\text{off}} < 120 \text{ s}^{-1}$  (Supporting Information Figure S6). Therefore, assuming a diffusion limited on a rate of  $10^9 \text{ M}^{-1} \text{ s}^{-1}$ , a dissociation constant  $K_{\text{d}} < 120 \text{ nM}$  can be estimated, thus in close agreement with the DELFIA and ITC data.

Recently, we reported that dimerization of 123B9 resulted in an agent with dramatically increased activity in the cell, presumably by facilitating receptor dimerization, and subsequent clustering and internalization.<sup>28</sup> Hence, we prepared a dimeric version of 135G3, namely 135G4, and a dimeric version of 135H11, namely 135H12 (Table 2 and Supporting Information Figure S1). On the basis of previous experience with dimeric agents, we did not expect that these agents would display increased affinity for the isolated EphA2-LBD (Table 2). However, we expected that ligand dimerization would result in increased receptor activation activity of the agent in cellular assays, presumably by facilitating receptor dimerization and subsequent clustering.

### Cellular Activity of the Novel EphA2 Agonistic Agents.

To assess whether optimized agents have retained their ability to function as EphA2 agonists, we first measured the ability of each agonistic agent to induce EphA2 receptor degradation. Both dimeric agents 135G4 and 135H12 were remarkably active in inducing receptor degradation and dephosphorylation of Ser897-EphA2 at submicromolar concentrations. However, in agreement with the relatively increased affinity of 135H11 compared to 135G3, their corresponding dimers displayed differential receptor activation, with 135H12 causing receptor degradation at nanomolar concentrations (Figure 4A).

Next, we examined the ability of 135H12 to reduce prooncogenic pSer897-EphA2 and to degrade EphA2 in pancreatic cancer cell lines BxPC3 and PANC-1. Western blot studies showed that 135H12 was able to degrade total EphA2 more effectively than the monomer 135H11 and YSA (Figure 4B). Moreover, to study the kinetics of EphA2 dephosphorylation and degradation upon 135H12 treatment, we treated BxPC3 cells with  $1 \mu\text{M}$  135H12 at different time points (Figure 4C). Western blot analysis indicated that total EphA2 was reduced after 10 min and totally diminished after 1 h of 135H12 treatment. Finally,

immunofluorescence data of BxPC3 cells demonstrated punctuated cytoplasmic EphA2 fluorescence in 135H12 treated cells compared to fluorescence localized at the cell membrane in 135H11 treated and untreated cells (Figure 4D). These results confirmed the increased agonistic activity of dimeric EphA2 ligands compared to their monomers.

Finally, to examine whether our improved EphA2 agonistic agents prevent cell migration and invasion of cancer cells, we performed cell migration and invasion assays using the scratch wound method as detected with an IncuCyte S3 (Sartorius) and the pancreatic cancer cell line BxPC3. In this assay, a 96-pin mechanical device (WoundMaker, Sartorius) was used to create homogeneous scratch wounds per plate, and the rate of wound closure between migrating (through a surface) and invading (through a Matrigel matrix) cells is directly observed in presence and absence of test ligands. The data revealed that 135H12 at 2.5  $\mu\text{M}$  concentration is very effective in suppressing both cell migration and invasion (Figure 5). However, and notably, while the dimer is more potent in suppressing cell migration, the monomer is equally effective in suppressing cell invasion (Figure 5 and Supporting Information Figure S3). These data conclude that 135H11 and 135H12 are potent agonistic EphA2 agents with nanomolar affinity for the receptor *in vitro* and low micromolar cellular activity.

## DISCUSSION

Recently, several accounts clearly identified EphA2 as a potential major target for novel and effective anticancer therapies. However, research in this field remains hampered by the lack of suitable, highly potent, and selective pharmacological tools that could provide stepping stones for the development of novel therapeutics.<sup>37</sup> The YSA peptide, discovered using phage display techniques, has been used in numerous applications, ranging from PDCs to incorporation in nanoparticles for delivery of diagnostics or siRNA. However, we recently reported that this peptide possessed relatively low *in vitro* affinity ( $\text{IC}_{50}$  15  $\mu\text{M}$ , Table 1) and required a triple-digit micromolar concentration in cell-based assays to activate the receptor. In addition, we found that the YSA peptide was fairly unstable in plasma with rapid hydrolysis by amino-peptidases.<sup>30,38</sup> Recently, we derived the agent 123B9, replacing the first Tyr residue with a 4F,3Cl phenylacetic acid and substituting two methionine residues in YSA with more stable residues, attaining only a modest increase in affinity ( $\text{IC}_{50}$  6.5  $\mu\text{M}$ , Table 1) but greatly improving the compound resistance to plasma proteases.<sup>30</sup> Here, by aligning the sequences of the *ephrin-A* ligands and the binding loop from a specific EphA2 antibody (1C1), and by systematically introducing non-natural amino acids, we attempted to derive novel and more potent agents. These data, summarized in Table 1, resulted in the identification first of agent 135E2 and subsequently of agent 135G3 with  $\text{IC}_{50}$  ~ 600 nM in a displacement assay and a dissociation constant of ~760 nM by isothermal titration calorimetry (Figure 1). In agreement with these increased affinities *in vitro*, the agents were more effective in cellular assays as shown in Figure 1E, where we observed that 135G3 displayed remarkably increased cellular activity in inducing tyrosine receptor phosphorylation compared to YSA (Figure 1E). Subsequently, we were able to obtain cocrystals of the complex between 135E2 and EphA2-LBD. The structure revealed several critical features that were then used to derive novel and even more potent agents. The bound conformation presented several features that were in agreement with the structure–activity

relationships reported in Table 1. For example, the C-terminal Arg residue is involved in a salt bridge with EphA2 residue Glu40, while the increased activity of the 5-hydroxyproline may be due to the formation of a hydrogen bond between this residue and Asp 43 (Figure 2A,C). Also, the peptide assumed a bent conformation that can be stabilized by introducing a covalent bridge or hydrophobic residues in lieu of residues Ser2 and Ser5 resulting in an entropy-driven increase in affinity (for example, compound 135G10, Table 2, Figure 3). Further modifications of the agent followed structure-based design strategies and resulted in the identification of a 2-benzofuranoic acid at position 1 that was predicted to introduce additional hydrogen bonding with EphA2 residue Arg103 (Figure 3B). In agreement, compound 135H11 displayed increased affinity in the nanomolar range both by DELFIA ( $IC_{50}$  0.15  $\mu$ M, Table 2) and by ITC ( $K_d$  = 0.16  $\mu$ M, Figure 3D). Finally, we prepared a dimeric version of 135G3 and 135H11, namely, 135G4 and 135H12, respectively, and evaluated their ability to induce receptor activation and to impair EphA2 pro-oncogenic signaling in pancreatic cancer cell lines (Figure 4). First, and in agreement with the increased affinity of 135H11 compared to 135G3, in our *in vitro* displacement assay and thermodynamic measurements, its dimer, 135H12, was remarkably and significantly more potent in degrading the receptor than 135G4 in pancreatic cancer cells (Figure 4A). In addition, both 135H11 and its dimeric version 135H12 were orders of magnitude more effective than 123B9 in causing EphA2 degradation and suppressing oncogenic pSer897-EphA2 in pancreatic cancer cell lines (Figure 4B,C). In agreement with these properties, the agents were also remarkably effective in suppressing both cell migration and invasion in a pancreatic cancer cell line (Figure 5). Interestingly, while both 135H11 and its dimer 135H12 were equally effective in suppressing cell invasion at low micromolar concentration, the dimer was significantly more effective in suppressing also cell migration (Figure 5, Supporting Information Figure S3). These data concluded that 135H12 represents a novel potent and effective pharmacological tool that can be further used to interrogate the role of EphA2 in tumorigenesis and cancer progression and metastasis.

The design of potent, selective, and effective agonistic small molecules or peptide mimetics targeting the ligand binding domain of the EphA2 receptor has remained a challenging task, despite several strategies that have been applied over the past decade ranging from NMR-based screening<sup>39–41</sup> and computational docking strategies<sup>21,42–44</sup> to high-throughput<sup>45</sup> and phage display screening.<sup>46</sup> More recently, studies have emerged with potential small molecule compounds<sup>21,42,28</sup> or EphA2/ephrin antagonists;<sup>43–45,47–49</sup> however, in our opinion, none of these agents have yet reached the level of potency and cellular efficacy that we reported here for 135H11 or 135H12. Indeed, the ability of the previously reported agents to cause receptor activation and internalization required relatively high concentrations (>50–100  $\mu$ M),<sup>46,50–52,28</sup> limiting their potential translation to the clinic as effective anti-pro-oncogenic EphA2 agents.

As we demonstrated recently, small agonistic peptides can be used directly as PDCs (peptide drug conjugates) to selectively deliver a cytotoxic agent to EphA2-expressing cancer cells.<sup>28,30,38,50,52,53</sup> Indeed, we envision that 135H11, 135H12, and related compounds (including, for example, the cyclic agent 135I4, Table 1) could be used as drug delivery agents for chemotherapy and could also be deployed to selectively introduce siRNA into cancer cells or appropriately derivatized with imaging or other diagnostic agents.<sup>52,54–57</sup>

However, given the remarkable activity of 135H12 inducing EphA2 degradation in the cell, and concomitant inhibition of cell migration and invasion, we anticipate that 135H12 and related compounds could be also used directly as single agents or in combination therapy against a variety of tumors that depend on EphA2 expression to metastasize. Hence, in addition to its anticipated use in PDCs or in diagnostics as we previously reported,<sup>28,30,38,50,52,53</sup> we envision performing further and more detailed pharmacology studies to evaluate the *in vivo* pharmacokinetics, toxicity, and efficacy of 135H12 and related compounds as single agents or in combination with the standard of care. In conclusion, we are confident that our present studies provide novel, potent, and effective pharmacological tools targeting the EphA2 receptor and as such represent a significant advancement in the field of targeting EphA2. Our studies could open a wide range of opportunities for the development of EphA2-targeting therapeutics, ranging from more effective PDCs to the development of innovative diagnostics, or for devising more effective combination therapies targeting tumor resistance to chemotherapy and tumor metastases.

## METHODS

### Chemistry.

**General.**—All reagents and anhydrous solvents were obtained from commercial sources, including Fmoc-protected amino acids and resins for solid phase synthesis. Some of the reported agents were synthesized by Innopep, while others were synthesized in house by standard microwave-assisted Fmoc peptide synthesis protocols on Rink amide resin using a Liberty Blue Peptide Synthesizer (CEM). For each coupling reaction, 6 equiv of Fmoc-AA, 3 equiv of DIC, and 1 equiv of OximaPure in 4.5 mL of DMF were used. The coupling reaction was allowed to proceed for 5 min at 90 °C in the microwave reactor. Fmoc deprotection was performed by treating the resin-bound peptide with 20% piperidine in DMF (2 × 3 mL) for 3 min at 90 °C. Peptides were cleaved from the resin with a cleavage cocktail containing TFA/TIS/water/phenol (94:2:2:2) for 3 h. The cleaving solution was filtered from the resin, and the peptides were precipitated in Et<sub>2</sub>O, centrifuged, and dried in a high vacuum. The crude peptides were purified to >95% purity by preparative RP-HPLC using a Luna C18 column (Phenomenex) on a JASCO preparative HPLC system and water/acetonitrile gradient (5% to 70%) containing 0.1% TFA. Compounds were further characterized by HRMS (Supporting Information Table S2).

**Preparation of 135G4 and 135H12.**—Dimers were prepared using half the resin needed for a normal scale reaction (usually 0.1 mmol) and introducing an Fmoc-Lys(Fmoc)-OH as the first amino acid of the sequence as illustrated in Supporting Information Figure S1. A double coupling protocol was employed to ensure the complete reaction of both elongating sequences. Standard cleavage and purification protocol were used to obtain the pure dimers (purity >95% by HPLC).

### Binding and Displacement Assays.

EphA2-LBD and EphA4-LBD were expressed and purified as we previously reported.<sup>30</sup> Isothermal Titration Calorimetry (ITC) measurements were obtained with a TA Instruments microcalorimeter. The optimized DELFIA (Dissociation-Enhanced Lanthanide Fluorescent

Immunoassay) assay protocol included a 2 h incubation of 100  $\mu\text{L}$  of 1  $\mu\text{M}$  123B9-biotin in 96-well streptavidin-coated plates (PerkinElmer), followed by three washing steps. Subsequently, after preincubation of test agents for 15 min with a solution of 0.712  $\mu\text{M}$  EphA2-LBD, 11  $\mu\text{L}$  of this mixture was added to 89  $\mu\text{L}$  of solution containing 4.17 nM Eu-N1-labeled anti-6XHis antibody (PerkinElmer) and incubated for 1 h. After washing steps, 200  $\mu\text{L}$  of the DELFIA enhancement solution (PerkinElmer) was added to each well followed by a 10 min incubation prior to fluorescence reading (VICTOR X5 microplate reader, PerkinElmer; excitation and emission wavelengths of 340 and 615 nm, respectively). Fluorescence readings were normalized to that of DMSO control and reported as percent inhibition. The  $\text{IC}_{50}$  values were analyzed using GraphPad Prism version 7 and data fitted with a nonlinear regression (least-squares ordinary fit) of the log-[compound] versus the observed response.

### Crystallization, X-ray Data Collection, and Structure Determination.

The EphA2 protein sample was mixed with the peptide in a 1:2 molar ratio for complex formation. Initial crystallization conditions were identified through sparse-matrix screening (Hampton Research Inc.). The crystals were subsequently reproduced using the hanging-drop vapor diffusion method at 4  $^{\circ}\text{C}$ , from drops mixed from 1  $\mu\text{L}$  of protein complex and 1  $\mu\text{L}$  of precipitant solution (0.1 M Tris-Cl, pH 8.0, 1.4–1.8 M  $\text{Li}_2\text{SO}_4$ ). Crystals were soaked for a few seconds in a cryo-protectant solution, composed of crystallization solution and 20% glycerol, before flash freezing in liquid nitrogen.

The X-ray diffraction data for the EphA2-LBD-135E2 peptide complex were collected on the BL 5.0.1 beamline at the Advanced Light Source, Lawrence Berkeley National Laboratory. The diffraction data were indexed, integrated and scaled using the HKL2000 program.<sup>31</sup> The structure was solved using the molecular replacement method in PHASER,<sup>32</sup> with the structure of free EphA2 (PDB ID: 3C8X) as a search model. The resulting electron density revealed that there are four EphA2-135E2 peptide complexes in each asymmetric unit, with one peptide containing AHHHHA. The structure of the complex was improved by iterative model building and refinement with Coot<sup>33</sup> and PHENIX software packages.<sup>34</sup> The same R-free test set was used throughout the refinement. The statistics for data collection and structural refinement of the complex EphA2-peptide are reported in Supporting Information Table S1.

### Cell Lines, Cell Culture, and Antibodies.

BxPC-3, PANC-1, and HEK273 T/17 (HEK293) cell lines were purchased from the American Type Culture Collection (ATCC). All culture media and supplements were purchased from ThermoFisher and supplemented with 10% FBS and 1% Pen Strep to make complete media. BxPC3 was cultured in complete RPMI-1640, and PANC-1 and HEK293 were cultured in complete DMEM. Anti-EphA2 antibody (1C11A12) was purchased from ThermoFisher, and anti-pS897-EphA2 antibody (D9A1) was purchased from Cell Signaling Technology. Both antibodies were probed at 1:1000 dilution.  $\beta$ -Actin antibody was purchased from Santa Cruz Biotechnology and probed at 1:10 000.

### EphA2 Stimulation and Immunoprecipitation.

We established an EphA2-overexpressing HEK293 stable cell line as we recently reported.<sup>28</sup> The EphA2 cell line was plated in six-well plates. The following day, cells were starved by replacing complete media with serum-free DMEM for 2 h. Starved cells were stimulated with 0.5–1  $\mu\text{g}/\text{mL}$  clustered mouse EphrinA1-Fc or Fc (R&D systems) with goat antihuman IgG Fc (Abcam, cat. no. ab97221) at various time points. During stimulation, indicated doses of compounds were added to each well. Control cells were treated with complete media containing 1% DMSO. Stimulated cells were lysed with cell lysis buffer (20 mM Tris, pH 7.4, 120 mM NaCl, 1% Triton X-100, 0.5% sodium deoxycholate, 0.1% SDS, 1% IGEPAL, 5 mM EDTA, supplemented with EDTA-free Protease Inhibitor Cocktail and PhosStop from Sigma-Aldrich) for 30 min on ice. Cell lysates were then centrifuged to clear off cell debris for 10 min at 13 000 rpm at 4 °C. Protein concentration was quantified using a BCA Protein Assay kit (ThermoFisher), and the sample concentration was adjusted to 1  $\mu\text{g}/\mu\text{L}$  for all samples. A preclear step for cell lysates was performed using Pierce Protein A/G Agarose beads (ThermoFisher) for 1 h at 4 °C. Cell lysates and beads were centrifuged, and the supernatant was further incubated with 2  $\mu\text{g}$  of mouse antibody anti-EphA2 receptor (ThermoFisher, cat. no. 1C11A12) at 4 °C overnight. The next day, each cell lysate–antibody complex was incubated with A/G agarose beads for 2 h at RT. After several washes, target protein was eluted by heating in 2X NuPAGE LDS Sample Buffer and NuPAGE Antioxidant (ThermoFisher) for 5 min at 90 °C. Samples were loaded into 4–12% NuPAGE Bis-Tris Precast Gels and transferred to PVDF membrane. The membrane was blocked with 5% BSA in TBS and 0.1% Tween (TBST) for 1 h, then incubated with a 1:3000 dilution of a mouse antibody anti-phosphotyrosine (BD Biosciences, cat. no. 610000, clone PY20) for 1 h. The antigen–antibody complex was visualized using a Clarity Western ECL kit (BIO-RAD). The membrane was washed and stripped using Restore Western Blot Stripping Buffer for 1 h, and subsequently blocked with 5% nonfat milk in TBST, followed by a 1 h incubation with a primary mouse antibody anti-EphA2 receptor at a 1:2000 dilution. The membrane was then washed with TBST and incubated with goat antimouse HRP.

### Immunofluorescence.

In chamber slides, cells were plated and allowed to adhere overnight in humidified cell culture incubators. The following day, cells were treated with the indicated ligands for 30 min. Subsequently, cells were washed with PBS and fixed with 4% formaldehyde (Polysciences, Inc.), then blocked and permeabilized with 5% FBS and 0.3% Triton X-100 for 1 h. Next, wells were washed and stained with anti-EphA2 antibody, followed by three washes and further incubation with Alexafluor goat antimouse 488 secondary antibody (ThermoFisher). Cells were counterstained with DAPI and mounted with Prolong Diamond Antifade (ThermoFisher). Images were acquired with confocal microscope Zeiss 880 Airyscan and processed using Adobe Photoshop CC.

### Time-Lapse Scratch Wound Healing Assays.

**Cell Migration Assay.**—Cells were cultured in 96-well ImageLock plates (Sartorius). The next day, wells were scratched using the WoundMaker (Sartorius). Subsequently, cells were washed twice with PBS and treated with the indicated compounds in RPMI-1640 complete

media. Subsequently, cells were imaged every 6 h using IncuCyte S3 (Sartorius), and relative wound areas were analyzed using the algorithm of the imager cell migration software module.

**Cell Invasion Assay.**—Matrigel (Corning) was diluted in serum-free RPMI-1640 media (1:100); 50  $\mu\text{L}$  of the mixture was added to an ImageLock plate and incubated at 37 °C for 2 h. Next, excess media were aspirated, and cells in complete media were plated and left overnight in a humidified cell culture incubator. The following day, the cell culture plate was aspirated, scratched with the WoundMaker, and washed twice with PBS. Subsequently, the plate was coated with a mixture of Matrigel and cold serum-free RPMI-1640 (1:1) and left in the incubator to solidify for 30 min. Finally, 100  $\mu\text{L}$  of 1.5X compound–media mixture was added to the plate at various concentrations. The healing of the scratches was imaged and calculated similar to the migration assay.

## Supplementary Material

Refer to Web version on PubMed Central for supplementary material.

## ACKNOWLEDGMENTS

Financial support was obtained in part by the NIH, with NCI grant CA168517. M.P. holds the Daniel Hays Chair in Cancer Research at the School of Medicine at University of California, Riverside. P.U. is a recipient of the 2017-2018 Pease Cancer Fellowship and of the 2018-2019 Burden Fellowship through the Division of Biomedical Sciences, School of Medicine at University of California, Riverside. J.S. is supported by the NIH (1R35GM119721) and March of Dimes Foundation (1-FY15-345). Some of the structural figures were prepared with the UCSF Chimera modeling package (<http://www.cgl.ucsf.edu/chimera>). Chimera is developed by the Resource for Biocomputing, Visualization, and Informatics at the University of California, San Francisco (supported by NIGMS P41-GM103311). Small amounts of 135H11, 135H12, or any of the reported agents can be obtained free of charge, for research purposes, upon request and signing of a standard material transfer agreement.

## ABBREVIATIONS

<b>EphA2-LBD</b>	ephrin type-A receptor 2 ligand-binding domain
<b>ITC</b>	isothermal titration calorimetry
<b>PET</b>	positron emission tomography
<b>MRI</b>	magnetic resonance imaging
<b>Hyp</b>	L- <i>trans</i> -4-hydroxyproline
<b>Aib</b>	$\alpha$ -aminoisobutyric acid
<b>Dap</b>	diamino propionic acid
<b>4 Pal</b>	4-pyridyl-L-alanine
<b>Cha</b>	3-cyclohexyl-L-alanine
<b>Nle</b>	L-norleucine
<b>hS</b>	L-homoserine

<b>hC</b>	L-homo-Cysteine
<b>3FABu</b>	(2S)-2-amino-4,4,4-trifluorobutanoic acid
<b>AspTtz</b>	2-amino-3-(2H-1,2,3,4-tetrazol-5-yl)propanoic acid

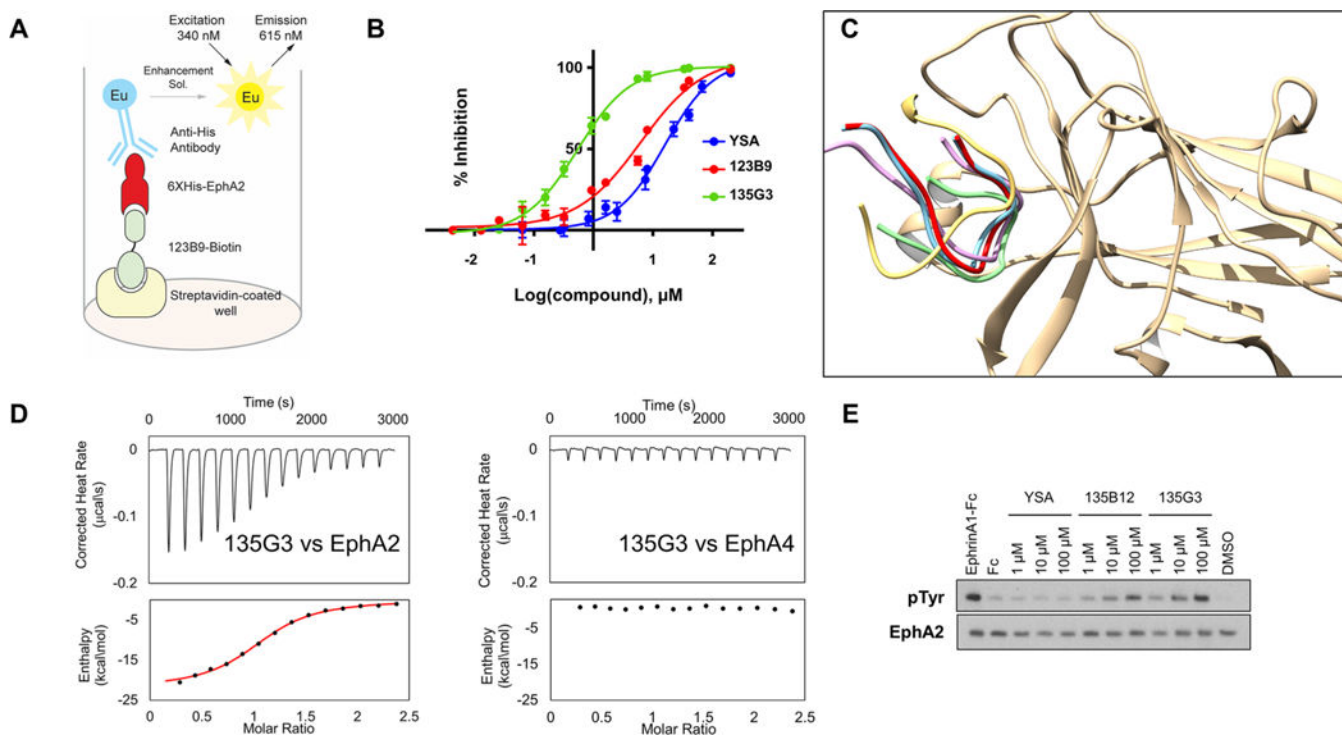
## REFERENCES

- (1). Hess AR, Seftor EA, Gardner LM, Carles-Kinch K, Schneider GB, Seftor RE, Kinch MS, and Hendrix MJ (2001) Molecular regulation of tumor cell vasculogenic mimicry by tyrosine phosphorylation: role of epithelial cell kinase (Eck/EphA2). *Cancer Res.* 61, 3250–3255. [PubMed: 11309274]
- (2). Walker-Daniels J, Coffman K, Azimi M, Rhim JS, Bostwick DG, Snyder P, Kerns BJ, Waters DJ, and Kinch MS (1999) Overexpression of the EphA2 tyrosine kinase in prostate cancer. *Prostate* 41, 275–280. [PubMed: 10544301]
- (3). Zeng G, Hu Z, Kinch MS, Pan CX, Flockhart DA, Kao C, Gardner TA, Zhang S, Li L, Baldrige LA, Koch MO, Ulbright TM, Eble JN, and Cheng L (2003) High-level expression of EphA2 receptor tyrosine kinase in prostatic intraepithelial neoplasia. *Am. J. Pathol.* 163, 2271–2276. [PubMed: 14633601]
- (4). Margaryan NV, Strizzi L, Abbott DE, Seftor EA, Rao MS, Hendrix MJ, and Hess AR (2009) EphA2 as a promoter of melanoma tumorigenicity. *Cancer Biol. Ther.* 8, 279–288. [PubMed: 19223760]
- (5). Abraham S, Knapp DW, Cheng L, Snyder PW, Mittal SK, Bangari DS, Kinch M, Wu L, Dhariwal J, and Mohammed SI (2006) Expression of EphA2 and Ephrin A-1 in carcinoma of the urinary bladder. *Clin. Cancer Res.* 12, 353–360. [PubMed: 16428472]
- (6). Ogawa K, Pasqualini R, Lindberg RA, Kain R, Freeman AL, and Pasquale EB (2000) The ephrin-A1 ligand and its receptor, EphA2, are expressed during tumor neovascularization. *Oncogene* 19, 6043–6052. [PubMed: 11146556]
- (7). Merritt WM, Thaker PH, Landen CN Jr., Deavers MT, Fletcher MS, Lin YG, Han LY, Kamat AA, Gershenson DM, Kinch MS, and Sood AK (2006) Analysis of EphA2 expression and mutant p53 in ovarian carcinoma. *Cancer Biol. Ther.* 5, 1357–1360. [PubMed: 16969087]
- (8). Duxbury MS, Ito H, Zinner MJ, Ashley SW, and Whang EE (2004) Ligation of EphA2 by Ephrin A1-Fc inhibits pancreatic adenocarcinoma cellular invasiveness. *Biochem. Biophys. Res. Commun.* 320, 1096–1102. [PubMed: 15249202]
- (9). Duxbury MS, Ito H, Zinner MJ, Ashley SW, and Whang EE (2004) EphA2: a determinant of malignant cellular behavior and a potential therapeutic target in pancreatic adenocarcinoma. *Oncogene* 23, 1448–1456. [PubMed: 14973554]
- (10). Mudali SV, Fu B, Lakkur SS, Luo M, Embuscado EE, and Iacobuzio-Donahue CA (2007) Patterns of EphA2 protein expression in primary and metastatic pancreatic carcinoma and correlation with genetic status. *Clin. Exp. Metastasis* 23, 357–365.
- (11). Wang LF, Fokas E, Bieker M, Rose F, Rexin P, Zhu Y, Pagenstecher A, Engenhardt-Cabillic R, and An HX (2008) Increased expression of EphA2 correlates with adverse outcome in primary and recurrent glioblastoma multiforme patients. *Oncol. Rep.* 19, 151–156. [PubMed: 18097589]
- (12). Wykosky J, Gibo DM, Stanton C, and Debinski W (2005) EphA2 as a novel molecular marker and target in glioblastoma multiforme. *Mol. Cancer Res.* 3, 541–551. [PubMed: 16254188]
- (13). Binda E, Visioli A, Giani F, Lamorte G, Copetti M, Pitter KL, Huse JT, Cajola L, Zanetti N, DiMeco F, De Filippis L, Mangiola A, Maira G, Anile C, De Bonis P, Reynolds BA, Pasquale EB, and Vescovi AL (2012) The EphA2 receptor drives self-renewal and tumorigenicity in stem-like tumor-propagating cells from human glioblastomas. *Cancer Cell* 22, 765–780. [PubMed: 23238013]
- (14). Miyazaki T, Kato H, Fukuchi M, Nakajima M, and Kuwano H (2003) EphA2 overexpression correlates with poor prognosis in esophageal squamous cell carcinoma. *Int. J. Cancer* 103, 657–663. [PubMed: 12494475]

- (15). Faoro L, Singleton PA, Cervantes GM, Lennon FE, Choong NW, Kanteti R, Ferguson BD, Husain AN, Tretiakova MS, Ramnath N, Vokes EE, and Salgia R (2010) EphA2 mutation in lung squamous cell carcinoma promotes increased cell survival, cell invasion, focal adhesions, and mammalian target of rapamycin activation. *J. Biol. Chem.* 285, 18575–18585. [PubMed: 20360610]
- (16). Yuan WJ, Ge J, Chen ZK, Wu SB, Shen H, Yang P, Hu B, Zhang GW, and Chen ZH (2009) Overexpression of EphA2 and EphrinA-1 in human gastric adenocarcinoma and its prognostic value for postoperative patients. *Dig. Dis. Sci.* 54, 2410–2417. [PubMed: 19101799]
- (17). Takahashi Y, Itoh M, Nara N, and Tohda S (2014) Effect of EPH-ephrin signaling on the growth of human leukemia cells. *Anticancer Res.* 34, 2913–2918. [PubMed: 24922654]
- (18). Trinidad EM, Zapata AG, and Alonso-Colmenar LM (2010) Eph-ephrin bidirectional signaling comes into the context of lymphocyte transendothelial migration. *Cell adhesion & migration* 4, 363–367. [PubMed: 20400865]
- (19). Alonso-C LM, Trinidad EM, de Garcillan B, Ballesteros M, Castellanos M, Cotillo I, Munoz JJ, and Zapata AG. (2009) Expression profile of Eph receptors and ephrin ligands in healthy human B lymphocytes and chronic lymphocytic leukemia B-cells. *Leuk. Res.* 33, 395–406. [PubMed: 18819711]
- (20). Guan M, Liu L, Zhao X, Wu Q, Yu B, Shao Y, Yang H, Fu X, Wan J, and Zhang W (2011) Copy number variations of EphA3 are associated with multiple types of hematologic malignancies. *Clinical lymphoma, myeloma & leukemia* 11, 50–53.
- (21). Petty A, Myshkin E, Qin H, Guo H, Miao H, Tochtrop GP, Hsieh JT, Page P, Liu L, Lindner DJ, Acharya C, MacKerell AD Jr., Ficker E, Song J, and Wang B (2012) A small molecule agonist of EphA2 receptor tyrosine kinase inhibits tumor cell migration in vitro and prostate cancer metastasis in vivo. *PLoS One* 7, e42120.
- (22). Amato KR, Wang S, Hastings AK, Youngblood VM, Santapuram PR, Chen H, Cates JM, Colvin DC, Ye F, Brantley-Sieders DM, Cook RS, Tan L, Gray NS, and Chen J (2014) Genetic and pharmacologic inhibition of EPHA2 promotes apoptosis in NSCLC. *J. Clin. Invest.* 124, 2037–2049. [PubMed: 24713656]
- (23). Amato KR, Wang S, Tan L, Hastings AK, Song W, Lovly CM, Meador CB, Ye F, Lu P, Balko JM, Colvin DC, Cates JM, Pao W, Gray NS, and Chen J (2016) EPHA2 Blockade Overcomes Acquired Resistance to EGFR Kinase Inhibitors in Lung Cancer. *Cancer Res.* 76, 305–318. [PubMed: 26744526]
- (24). Miao B, Ji Z, Tan L, Taylor M, Zhang J, Choi HG, Frederick DT, Kumar R, Wargo JA, Flaherty KT, Gray NS, and Tsao H (2015) EPHA2 is a mediator of vemurafenib resistance and a novel therapeutic target in melanoma. *Cancer Discovery* 5, 274–287. [PubMed: 25542448]
- (25). Heinzlmeir S, Kudlinzki D, Sreeramulu S, Klaeger S, Gande SL, Linhard V, Wilhelm M, Qiao H, Helm D, Ruprecht B, Saxena K, Medard G, Schwalbe H, and Kuster B (2016) Chemical Proteomics and Structural Biology Define EPHA2 Inhibition by Clinical Kinase Drugs. *ACS Chem. Biol.* 11, 3400–3411. [PubMed: 27768280]
- (26). Petty A, Idippily N, Bobba V, Geldenhuys WJ, Zhong B, Su B, and Wang B (2018) Design and synthesis of small molecule agonists of EphA2 receptor. *Eur. J. Med. Chem.* 143, 1261–1276. [PubMed: 29128116]
- (27). Hasegawa J, Sue M, Yamato M, Ichikawa J, Ishida S, Shibusaki T, Kitamura M, Wada T, and Agatsuma T (2016) Novel anti-EPHA2 antibody, DS-8895a for cancer treatment. *Cancer Biol. Ther.* 17, 1158–1167. [PubMed: 27653549]
- (28). Salem AF, Wang S, Billet S, Chen JF, Udompholkul P, Gambini L, Baggio C, Tseng HR, Posadas EM, Bhowmick NA, and Pellecchia M (2018) Reduction of Circulating Cancer Cells and Metastases in Breast-Cancer Models by a Potent EphA2- Agonistic Peptide-Drug Conjugate. *J. Med. Chem.* 61, 2052–2061. [PubMed: 29470068]
- (29). Koolpe M, Dail M, and Pasquale EB (2002) An ephrin mimetic peptide that selectively targets the EphA2 receptor. *J. Biol. Chem.* 277, 46974–46979. [PubMed: 12351647]
- (30). Wu B, Wang S, De SK, Barile E, Quinn BA, Zharkikh I, Purves A, Stebbins JL, Oshima RG, Fisher PB, and Pellecchia M (2015) Design and Characterization of Novel EphA2 Agonists for Targeted Delivery of Chemotherapy to Cancer Cells. *Chem. Biol.* 22, 876–887. [PubMed: 26165155]

- (31). Otwinowski Z, and Minor W (1997) Processing of X-ray diffraction data collected in oscillation mode. *Methods Enzymol* 276, 307–326.
- (32). McCoy AJ, Grosse-Kunstleve RW, Adams PD, Winn MD, Storoni LC, and Read RJ (2007) Phaser crystallographic software. *J. Appl. Crystallogr.* 40, 658–674. [PubMed: 19461840]
- (33). Emsley P, and Cowtan K (2004) Coot: model-building tools for molecular graphics. *Acta Crystallogr., Sect. D: Biol. Crystallogr.* 60, 2126–2132. [PubMed: 15572765]
- (34). Adams PD, Grosse-Kunstleve RW, Hung LW, Ioerger TR, McCoy AJ, Moriarty NW, Read RJ, Sacchettini JC, Sauter NK, and Terwilliger TC (2002) PHENIX: building new software for automated crystallographic structure determination. *Acta Crystallogr., Sect. D: Biol. Crystallogr.* 58, 1948–1954. [PubMed: 12393927]
- (35). Khrapunov S (2018) The enthalpy-entropy compensation phenomenon. Limitations for the use of some basic thermodynamic equations. *Curr. Protein Pept. Sci.* 19, 1088–1091. [PubMed: 29779476]
- (36). Fox JM, Zhao M, Fink MJ, Kang K, and Whitesides GM (2018) The Molecular Origin of Enthalpy/Entropy Compensation in Biomolecular Recognition. *Annu. Rev. Biophys.* 47, 223. [PubMed: 29505727]
- (37). Lodola A, Giorgio C, Incerti M, Zanotti I, and Tognolini M (2017) Targeting Eph/ephrin system in cancer therapy. *Eur. J. Med. Chem.* 142, 152–162. [PubMed: 28780190]
- (38). Barile E, Wang S, Das SK, Noberini R, Dahl R, Stebbins JL, Pasquale EB, Fisher PB, and Pellicchia M (2014) Design, synthesis and bioevaluation of an EphA2 receptor-based targeted delivery system. *ChemMedChem* 9, 1403–1412. [PubMed: 24677792]
- (39). Wu B, De SK, Kulinich A, Salem AF, Koeppen J, Wang R, Barile E, Wang S, Zhang D, Ethell I, and Pellicchia M (2017) Potent and Selective EphA4 Agonists for the Treatment of ALS. *Cell Chem. Biol.* 24, 293–305. [PubMed: 28196613]
- (40). Wu B, Barile E, De SK, Wei J, Purves A, and Pellicchia M (2015) High-Throughput Screening by Nuclear Magnetic Resonance (HTS by NMR) for the Identification of PPIs Antagonists. *Curr. Top. Med. Chem.* 15, 2032–2042. [PubMed: 25986689]
- (41). Wu B, Zhang Z, Noberini R, Barile E, Giulianotti M, Pinilla C, Houghten RA, Pasquale EB, and Pellicchia M (2013) HTS by NMR of combinatorial libraries: a fragment-based approach to ligand discovery. *Chem. Biol.* 20, 19–33. [PubMed: 23352136]
- (42). Petty A, Idippily N, Bobba V, Geldenhuys WJ, Zhong B, Su B, and Wang B (2018) Design and synthesis of small molecule agonists of EphA2 receptor. *Eur. J. Med. Chem.* 143, 1261. [PubMed: 29128116]
- (43). Hassan-Mohamed I, Giorgio C, Incerti M, Russo S, Pala D, Pasquale EB, Zanotti I, Vicini P, Barocelli E, Rivara S, Mor M, Lodola A, and Tognolini M (2014) UniPR129 is a competitive small molecule Eph-ephrin antagonist blocking in vitro angiogenesis at low micromolar concentrations. *Br. J. Pharmacol.* 171, 5195–5208. [PubMed: 24597515]
- (44). Tognolini M, Incerti M, Pala D, Russo S, Castelli R, Hassan-Mohamed I, Giorgio C, and Lodola A (2014) Target hopping as a useful tool for the identification of novel EphA2 proteinprotein antagonists. *ChemMedChem* 9, 67–72. [PubMed: 24115725]
- (45). Giorgio C, Incerti M, Corrado M, Rusnati M, Chiodelli P, Russo S, Callegari D, Ferlenghi F, Ballabeni V, Barocelli E, Lodola A, and Tognolini M (2018) Pharmacological evaluation of new bioavailable small molecules targeting Eph/ephrin interaction. *Biochem. Pharmacol.* 147, 21. [PubMed: 29129483]
- (46). Mitra S, Duggineni S, Koolpe M, Zhu X, Huang Z, and Pasquale EB (2010) Structure-activity relationship analysis of peptides targeting the EphA2 receptor. *Biochemistry* 49, 6687–6695. [PubMed: 20677833]
- (47). Incerti M, Tognolini M, Russo S, Pala D, Giorgio C, Hassan-Mohamed I, Noberini R, Pasquale EB, Vicini P, Piersanti S, Rivara S, Barocelli E, Mor M, and Lodola A (2013) Amino acid conjugates of lithocholic acid as antagonists of the EphA2 receptor. *J. Med. Chem.* 56, 2936–2947. [PubMed: 23489211]
- (48). Castelli R, Tognolini M, Vacondio F, Incerti M, Pala D, Callegari D, Bertoni S, Giorgio C, Hassan-Mohamed I, Zanotti I, Bugatti A, Rusnati M, Festuccia C, Rivara S, Barocelli E, Mor M,

- and Lodola A (2015) Delta(5)-Cholenoyl -amino acids as selective and orally available antagonists of the Eph-ephrin system. *Eur. J. Med. Chem.* 103, 312–324. [PubMed: 26363867]
- (49). Tandon M, Vemula SV, and Mittal SK (2011) Emerging strategies for EphA2 receptor targeting for cancer therapeutics. *Expert Opin. Ther. Targets* 15, 31–51. [PubMed: 21142802]
- (50). Wang S, Placzek WJ, Stebbins JL, Mitra S, Noberini R, Koolpe M, Zhang Z, Dahl R, Pasquale EB, and Pellecchia M (2012) Novel targeted system to deliver chemotherapeutic drugs to EphA2-expressing cancer cells. *J. Med. Chem.* 55, 2427–2436. [PubMed: 22329578]
- (51). Duggineni S, Mitra S, Lamberto I, Han X, Xu Y, An J, Pasquale EB, and Huang Z (2013) Design and Synthesis of Potent Bivalent Peptide Agonists Targeting the EphA2 Receptor. *ACS Med. Chem. Lett.* 4, 344.
- (52). Wang S, Noberini R, Stebbins JL, Das S, Zhang Z, Wu B, Mitra S, Billet S, Fernandez A, Bhowmick NA, Kitada S, Pasquale EB, Fisher PB, and Pellecchia M (2013) Targeted delivery of paclitaxel to EphA2-expressing cancer cells. *Clin. Cancer Res.* 19, 128–137. [PubMed: 23155185]
- (53). Quinn BA, Wang S, Barile E, Das SK, Emdad L, Sarkar D, De SK, Morvaridi SK, Stebbins JL, Pandol SJ, Fisher PB, and Pellecchia M (2016) Therapy of pancreatic cancer via an EphA2 receptor-targeted delivery of gemcitabine. *Oncotarget* 7, 17103–17110. [PubMed: 26959746]
- (54). Patel AR, Chougule M, and Singh M (2014) EphA2 targeting pegylated nanocarrier drug delivery system for treatment of lung cancer. *Pharm. Res.* 31, 2796–2809. [PubMed: 24867421]
- (55). Xie X, Yang Y, Lin W, Liu H, Liu H, Yang Y, Chen Y, Fu X, and Deng J (2015) Cell-penetrating peptide-siRNA conjugate loaded YSA-modified nanobubbles for ultrasound triggered siRNA delivery. *Colloids Surf. B* 136, 641–650.
- (56). Cai W, Ebrahimnejad A, Chen K, Cao Q, Li ZB, Tice DA, and Chen X (2007) Quantitative radioimmunoPET imaging of EphA2 in tumor-bearing mice. *Eur. J. Nucl. Med. Mol. Imaging* 34, 2024–2036. [PubMed: 17673999]
- (57). Liu Y, Lan X, Wu T, Lang J, Jin X, Sun X, Wen Q, and An R (2014) (99m)Tc-labeled SWL specific peptide for targeting EphA2 receptor. *Nucl. Med. Biol.* 41, 450–456. [PubMed: 24768147]

**Figure 1.**

Design of 135G3. (A) Schematic representation of the DELFIA assay. (B) DELFIA displacement curves relative to YSA ( $\text{IC}_{50} = 16.5 \mu\text{M}$ ), 123B9 ( $\text{IC}_{50} = 6.5 \mu\text{M}$ ), and 135G3 ( $\text{IC}_{50} = 0.6 \mu\text{M}$ ) against the EphA2-LBD. (C) Close-up view of the structure of EphA2-LBD (light brown, PDB ID 3MX0) in complex with various ephrin ligands or the 1C1 antibody. Only the loop regions of the ligands are shown: ephrinA1 (light blue, 3CZU), ephrinA2 (purple, 2WO3), ephrinA4 (red, 3MX0), ephrinB2 (green, 1KGY), and the anti-EphA2 antibody 1C1 (yellow, 3SKJ). This figure panel was generated with Chimera (<http://www.cgl.ucsf.edu/chimera>). (D) Isothermal Titration Calorimetry (ITC) curves for the binding between 135G3 and EphA2-LBD ( $H = -21.9 \text{ kcal/mol}$ ,  $-T S = 13.5 \text{ kcal/mol}$ ) and EphA4-LBD (no appreciable binding). (E) EphA2 receptor phosphorylation assay in HEK293 cells by various doses of YSA, 123B9, and 135G3.

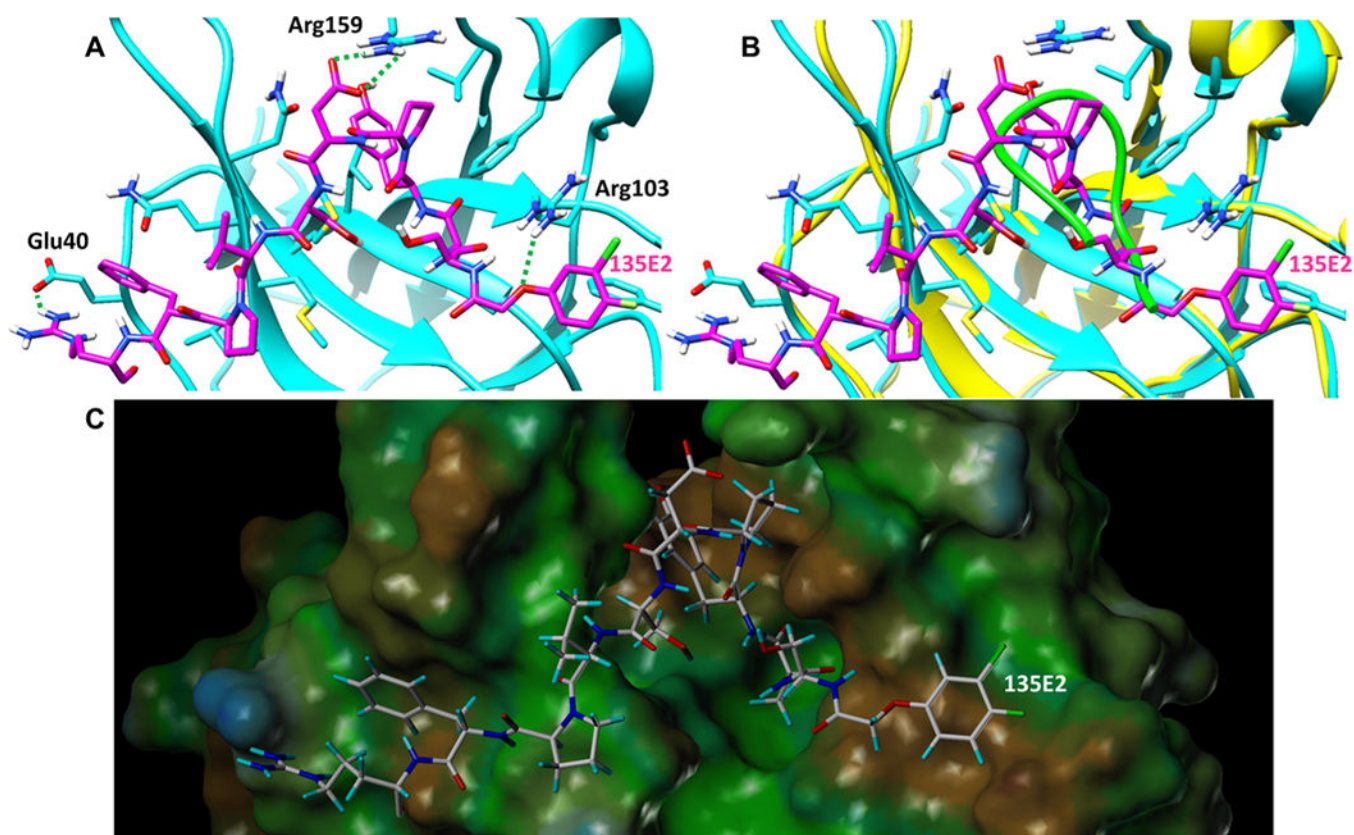


**Figure 2.** The X-ray structure of 135H2 in complex with the EphA2 LBD. (A) 135E2 is depicted as a stick model in magenta, while the EphA2 is depicted as a ribbon model and with several side chains that interact with the peptide displayed. (B) Superposition of the structures of 135H2 (stick model in magenta) in complex with EphA2-LBD (ribbon in cyan) and the complex between EphA2-LBD (ribbon model in yellow) and ephrinA5 (only the interacting loop region is shown as a green rod). (C) Detailed interactions between 135E2 (stick model) and EphA2-LBD (surface representation). The surface was generated with MOLCAD and colored according to a lipophilic potential (brown, more lipophilic; blue, more polar).

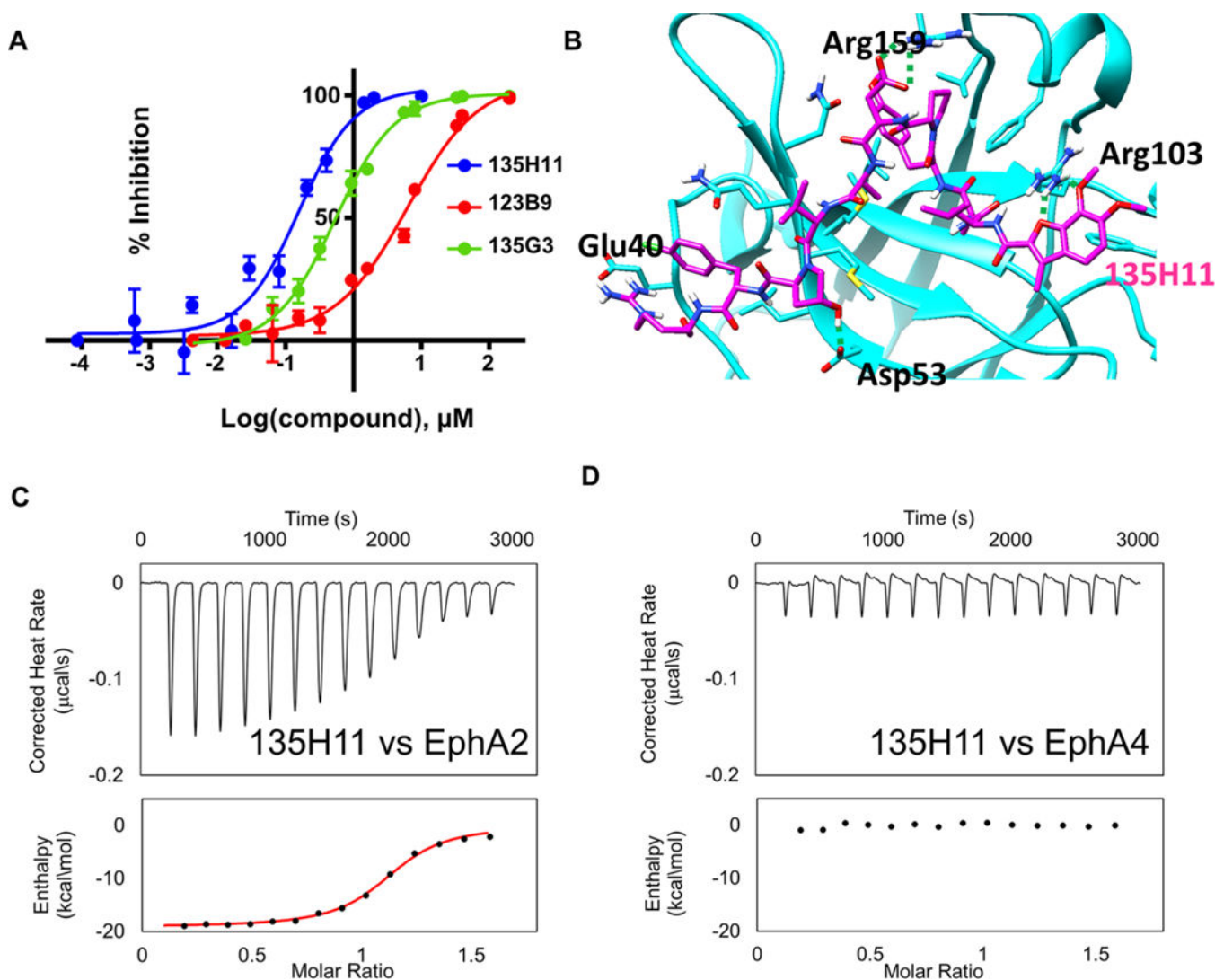


**Figure 3.**

Design and characterization of 135H11. (A) DELFIA displacement dose–response curves comparing 123B9, 135G3, and 135H11 (Table 2). (B) Model of the complex between 135H11 and EphA2-LBD. The model was obtained using Sybyl (Cetara) and our derived X-ray structure of the complex between 135H2 and EphA2-LBD (PDB ID 6B9L).

Intermolecular hydrogen bonding involving side chains is highlighted in green. (C) ITC curves for 135H11 against EphA2-LBD ( $K_d = 150 \text{ nM}$ ) and (D) EphA4-LBD (inactive).

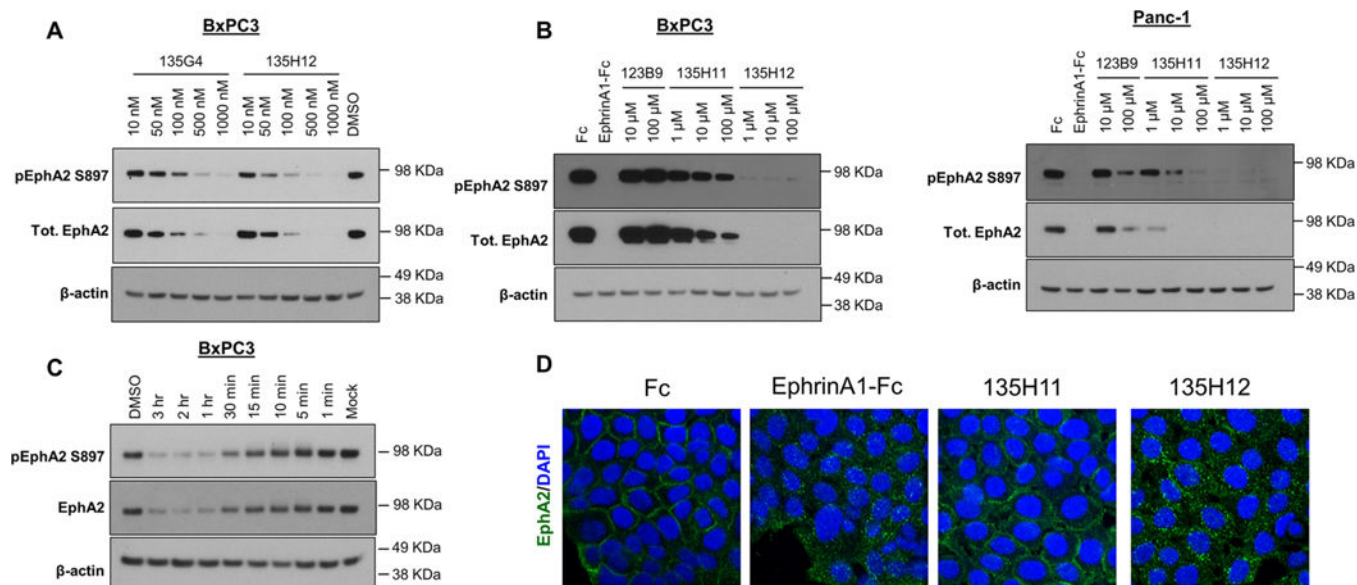


**Figure 4.**

Dimeric EphA2 agonists degrade EphA2 receptors in cancer cells. (A) Comparison studies between the two dimeric EphA2 agonists 135H12 and 135G4 in a cell-based assay. BxPC3 cell line was treated with the indicated doses for 3 h; then cells were lysed and Western blot studies were performed. Both dimers degraded total EphA2 receptor and dephosphorylated pEphA2 S897 at nanomolar concentrations, but 135H12 was more potent at lower doses compared to 135G4 (evident comparing the 50 nM and 100 nM treated lanes). (B) 135H12 was an effective agonist compared to EphA2 agonistic monomers. BxPC3 or PANC-1 cells were treated and lysed similar to the previous Western blot. 135H12 degraded total EphA2 receptor and dephosphorylated pEphA2 S897 at 1  $\mu$ M in both cell lines. Moreover, the monomer 135H11 was more effective than the monomer 123B9. EphrinA1-Fc is a clustered natural ligand and used as a positive control. (C) Kinetics of EphA2 degradation after treatment with 135H12 (1  $\mu$ M). BxPC3 cells were treated with 1  $\mu$ M 135H12 and cell lysates collected at the indicated time points and blotted with phospho-EphA2 S897 or EphA2. EphA2 receptor was dephosphorylated and degraded after 10 min of adding 135H12. Moreover, the receptor band disappeared after 1 h of treatment. (D) 135H12 altered EphA2 cellular localization. BxPC3 cells were plated in chamber slides, and the following day they were treated with clustered Fc, clustered EphrinA1, 1  $\mu$ M of 135H11, or 1  $\mu$ M 135H12 for 30 min. Cells were immunostained with EphA2 antibody (green), and nuclei were counterstained with DAPI (blue). Images were acquired using confocal Inverted Zeiss 880. The EphA2 receptor was located at the cell membrane when treated with Fc or 135H11. On the contrary, punctuated fluorescence was observed in the cytoplasm of ephrinA1-Fc and 135H12 treated cells, suggesting receptor clustering and internalization.

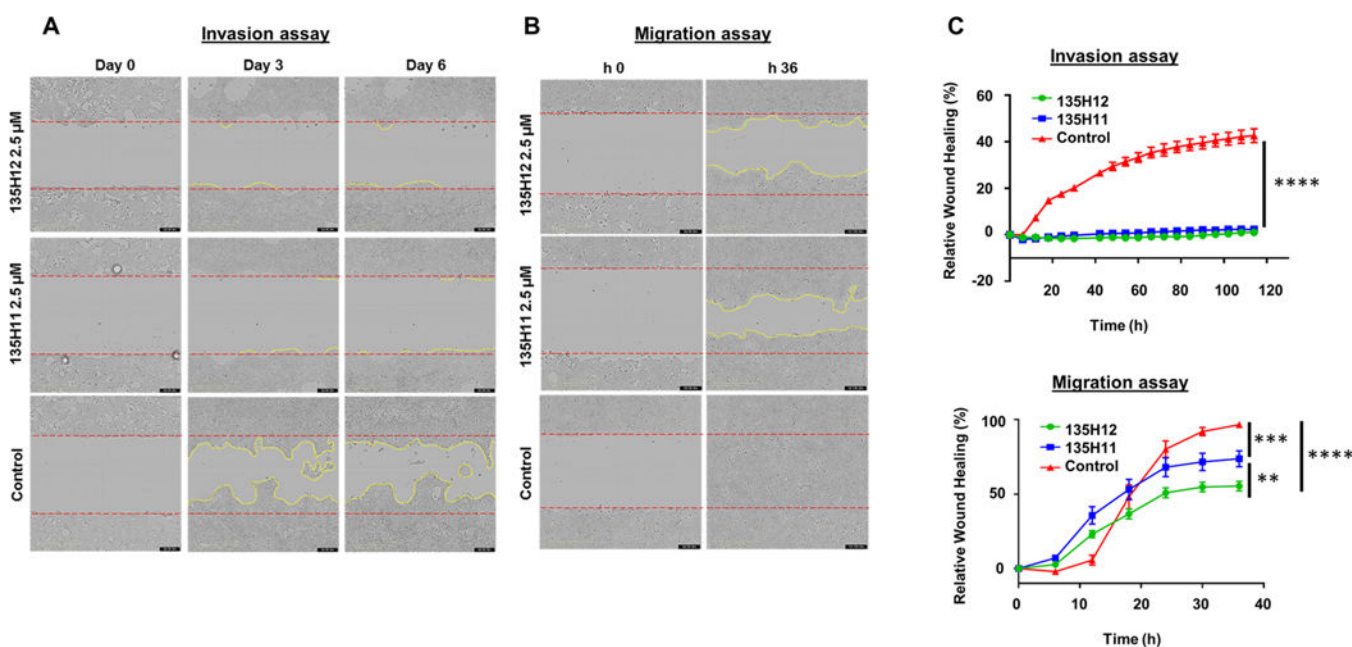


**Figure 5.**

EphA2 agonists inhibit cell invasion and migration. (A) 135H12 and 135H11 inhibit cell invasion. Seven  $\times 10^5$  BxPC3 cells were plated in each well of a 96-well plate and treated the following day. Plates were treated once and imaged every 6 h for 6 days. (B) 135H12 and 135H11 inhibit cell migration. BxPC3 cells were plated and treated similarly to the invasion assay. Plates were imaged every 6 h for 36 h. (C) Time dependent inhibition of invasion and migration of pancreatic cancer cells when treated with 135H11 (monomer) and 135H12 (dimer). Both agonists inhibited cell invasion, while 135H12 showed more significant inhibition of cell migration than its monomer counterpart, 135H11. Invasion assay  $n = 5$ , migration assay  $n = 10$ . Error bars are SEM \*\*\*\* $P = 0.0001$ ; \*\*\* $P = 0.0002$ ; \*\* $P = 0.003$ .

**Table 1.**Tested Agents and Relative IC<sub>50</sub> Values ( $\mu\text{M}$ ) from DELFIA Assay<sup>a</sup>

ID	sequence	IC <sub>50</sub> ( $\mu\text{M}$ )
YSA	H <sub>2</sub> N-YSAYPDSVPMMS-CONH <sub>2</sub>	16.2 ± 0.8, <i>n</i> = 14
123B9	(4-F,3-CIPhOCH <sub>2</sub> CO)SAYPDSVP(Nle)(hS)-CONH <sub>2</sub>	6.6 ± 1.0, <i>n</i> = 4
ephrins A2/A5/A4	H <sub>2</sub> N-FTPFSLGFVFRP-CONH <sub>2</sub>	>200
ephrin A3	H <sub>2</sub> N-YSAFSLGYEFHA-CONH <sub>2</sub>	>200
ephrin B2	H <sub>2</sub> N-FSPNLWGLEFQK-CONH <sub>2</sub>	>200
ephrin A1	H <sub>2</sub> N-FTPFTLGKEFKE-CONH <sub>2</sub>	>200
135A1 (1C1)	H <sub>2</sub> N-YDYVAVAGPAEY-CONH <sub>2</sub>	>500
135A7	H <sub>2</sub> N-YSAYPLSVEFRP-CONH <sub>2</sub>	>100
135A8	H <sub>2</sub> N-YSAYPDSVEFRP-CONH <sub>2</sub>	36.3 ± 6.2,
135B1	H <sub>2</sub> N-YSAYPDSVEMMS-CONH <sub>2</sub>	>100
135B12	H <sub>2</sub> N-YSAYPDSVDFRP-CONH <sub>2</sub>	1.9 ± 0.1, <i>n</i> = 22
135B2	H <sub>2</sub> N-YSAYPLSVEEMMS-CONH <sub>2</sub>	>200
135B8	H <sub>2</sub> N-FTAFLPLGFVFRP-CONH <sub>2</sub>	>100
135B9	H <sub>2</sub> N-FTAFLPLGFEMMS-CONH <sub>2</sub>	>100
135C1	H <sub>2</sub> N-YSAYPDSVDFMS-CONH <sub>2</sub>	7.5 ± 0.5
135C2	H <sub>2</sub> N-YSAYPDSVDF-CONH <sub>2</sub>	11.2 ± 1.4
135C3	H <sub>2</sub> N-YSAYPDSVDFRS-CONH <sub>2</sub>	4.4 ± 0.9
135C4	H <sub>2</sub> N-YSAYPDSVDFR-CONH <sub>2</sub>	4.9 ± 0.1
135C7	H <sub>2</sub> N-YSAYPDSVDMRS-CONH <sub>2</sub>	8.8 ± 0.1
135C8	H <sub>2</sub> N-YSAYPDSVDMRP-CONH <sub>2</sub>	8.4 ± 1.2
135C9	H <sub>2</sub> N-YSAYPDSVDMMP-CONH <sub>2</sub>	11.8 ± 0.4
135C10	H <sub>2</sub> N-YSAYPDSVDFMP-CONH <sub>2</sub>	4.6 ± 0.1
135D6	H <sub>2</sub> N-YSCYPDSVDFRP-CONH <sub>2</sub>	>100
135D7	H <sub>2</sub> N-YSVYPDSVDFRP-CONH <sub>2</sub>	>200
135D8	H <sub>2</sub> N-YSLYPDSVDFRP-CONH <sub>2</sub>	>200, <i>n</i> = 2
135D9	H <sub>2</sub> N-YS(Aib)YPDSVDFRP-CONH <sub>2</sub>	>200
135E2	(4-F,3-C1PhOCH <sub>2</sub> CO)SAYPDSVDFRP-CONH <sub>2</sub>	3.1 ± 0.4, <i>n</i> = 6
135E4	H <sub>2</sub> N-YSAYPDSVP(4-ClPhe)RP-CONH <sub>2</sub>	1.6 ± 0.2, <i>n</i> = 8
135E5	H <sub>2</sub> N-YSAYPDSVP(3-ClPhe)RP-CONH <sub>2</sub>	1.8 ± 0.1
135E6	H <sub>2</sub> N-YSAYPDSVP(4-FPhe)RP-CONH <sub>2</sub>	3.1 ± 0.4
135E7	H <sub>2</sub> N-YSAYPDSVP(4-CF <sub>3</sub> Phe)RP-CONH <sub>2</sub>	1.9 ± 0.2
135E10	H <sub>2</sub> N-YSAYPDSVPF(4-Amino-Phe)P-CONH <sub>2</sub>	2.3 ± 0.3
135E11	H <sub>2</sub> N-YSAYPDSVPF(4-Amino-Methyl-Phe)P-CONH <sub>2</sub>	1.3 ± 0.2
135E12	H <sub>2</sub> N-YSAYPDSVPF(4-Guanidino-Phe)P-CONH <sub>2</sub>	1.0 ± 0.1
135F1	H <sub>2</sub> N-YSAYPDSVPFKP-CONH <sub>2</sub>	1.5 ± 0.1
135F2	H <sub>2</sub> N-YSAY(Hyp)DSVDFRP-CONH <sub>2</sub>	14.5 ± 0.8

ID	sequence	IC <sub>50</sub> (μM)
135F3	H <sub>2</sub> N-YSAYPDSV(Hyp)FRP-CONH <sub>2</sub>	1.5 ± 0.1
135F4	H <sub>2</sub> N-YSAYPDSVPFR(Hyp)-CONH <sub>2</sub>	5.6 ± 0.5
135F5	H <sub>2</sub> N-YSA(4C1Phe)PDSVPFRP-CONH <sub>2</sub>	3.5 ± 0.3
135F6	H <sub>2</sub> N-YSA(3C1Phe)PDSVPFRP-CONH <sub>2</sub>	11.4 ± 1.3
135F8	H <sub>2</sub> N-YSAYPDSVP(4 Pa1)RP-CONH <sub>2</sub>	7.6 ± 0.1
135F10	H <sub>2</sub> N-YSAYPDSV(Hyp)(4C1Phe)RP-CONH <sub>2</sub>	0.94 ± 0.11, <i>n</i> = 6
135F12	(4F,3ClPhOCH <sub>2</sub> CO)SAYPDSVPFRP(β-Ala)K-CONH <sub>2</sub>	4.1 ± 0.1
135G3	(4F,3ClPhOCH <sub>2</sub> CO)SAYPDSV(Hyp)(4C1Phe)RP-CONH <sub>2</sub>	0.54 ± 0.03, <i>n</i> = 10
135C11	(H <sub>2</sub> N-YSAYPDSVPFRPG) <sub>2</sub> -K-CONH <sub>2</sub>	0.60 ± 0.09, <i>n</i> = 6

<sup>a</sup>SE represents duplicate measurements unless otherwise indicated. Hyp, L-trans-4-hydroxyproline; Aib, α-aminoisobutyric acid; 4 Pa1, 4-pyridyl-L-alanine; Nle, L-norleucine; hS, L-homo-serine

Table 2.

Novel EphA2-Targeting Agents and Relative IC<sub>50</sub> Values ( $\mu\text{M}$ )<sup>a</sup>

ID	sequence	IC <sub>50</sub> ( $\mu\text{M}$ )
135G8	H <sub>2</sub> N-Y( <u>C</u> AYPD <u>C</u> )VPFRP-CO <sub>2</sub> NH <sub>2</sub>	32.9 ± 10.9
135G9	H-Y( <u>E</u> AYPD <u>D</u> <u>ap</u> )VPFRP-NH <sub>2</sub>	27.2 ± 0.3
135I2	H <sub>2</sub> N-Y( <u>h</u> CAYPD <u>C</u> )VPFRP-CO <sub>2</sub> NH <sub>2</sub>	10.1 ± 0.1
135I3	H <sub>2</sub> N-Y( <u>C</u> AYPD <u>h</u> <u>C</u> )VPFRP-CO <sub>2</sub> NH <sub>2</sub>	1.2 ± 0.2
135F11	(4F,3-ClPhOCH <sub>2</sub> CO)(Dap)AYPDDVPFRP-CO <sub>2</sub> NH <sub>2</sub>	>200
135G10	(4F,3ClPhOCH <sub>2</sub> CO)LAYPDAV(Hyp)(4ClPhe)RP-CO <sub>2</sub> NH <sub>2</sub>	0.23 ± 0.08, n = 4
135G11	(4F,3ClPhOCH <sub>2</sub> CO)SA(4MeTyr)PDSV(Hyp)(4ClPhe)RP-CO <sub>2</sub> NH <sub>2</sub>	0.18 ± 0.05
135G12	(4F,3ClPhOCH <sub>2</sub> CO)SAYP(AspTtz)SV(Hyp)(4ClPhe)RP-CO <sub>2</sub> NH <sub>2</sub>	0.70 ± 0.09
135H2	(4F,3ClPhOCH <sub>2</sub> CO)(Cha)AYPDAV(Hyp)(4ClPhe)RP-CO <sub>2</sub> NH <sub>2</sub>	1.7 ± 0.1
135H3	(4F,3ClPhOCH <sub>2</sub> CO)LAYPD(3FABu)V(Hyp)(4ClPhe)RP-CO <sub>2</sub> NH <sub>2</sub>	11.2 ± 0.1
135H4	(4F,3ClPhOCH <sub>2</sub> CO)(Cha)AYPD(3FABu)V(Hyp)(4ClPhe)RP-CO <sub>2</sub> NH <sub>2</sub>	53.2 ± 8.5
135G6	XSAYPDSVPFRP-NH <sub>2</sub> X = 3,6-dimethyl- benzofuran-2-carboxylic acid	0.66 ± 0.01
135G5	XSAYPDSVPFRP-NH <sub>2</sub> X = 5-methyl- benzofuran-2-carboxylic acid	0.50 ± 0.05
135H5	XSAYPDSVPFRP-CO <sub>2</sub> NH <sub>2</sub> X = 3-methyl-5- fluoro-benzofuranoic acid	0.43 ± 0.01
135G7	XSAYPDSVPFRP-NH <sub>2</sub> X = 7-methoxy-2- benzofurancarboxylic acid	0.19 ± 0.04, n = 8
135H1	XSAYPDSV(Hyp)(4ClPhe)RP-CO <sub>2</sub> NH <sub>2</sub> X = 5-chloro-benzodihydrofuranoic acid	0.75 ± 0.04
135H6	XSAYPDSVPFRP-CO <sub>2</sub> NH <sub>2</sub> X = 3-methyl-5- chloro-benzofuranoic acid	0.19 ± 0.01
135H7	XSAYPDSVPFRP-CO <sub>2</sub> NH <sub>2</sub> X = 3-methyl-6,7- diethoxy-benzofuranoic acid	0.24 ± 0.02
135H8	XSAYPDSVPFRP-CO <sub>2</sub> NH <sub>2</sub> X = 7-ethoxy- benzofuranoic acid	0.17 ± 0.03
135H9	XSAYPDSVPFRP-CO <sub>2</sub> NH <sub>2</sub> X = 5-chloro-7- methoxy-benzofuranoic acid	0.28 ± 0.01
135H10	XSAYPDSVPFRP-CO <sub>2</sub> NH <sub>2</sub> X = 3-methyl-6,7- dimethoxy-benzofuranoic acid	0.19 ± 0.05, n = 6
135H11	XLA(4MeTyr)PDA V(Hyp)(4ClPhe)RP-CO <sub>2</sub> NH <sub>2</sub> X = 3-methyl-6,7-dimethoxy-benzofuranoic acid	0.13 ± 0.02, n = 6
135I4	X( <u>C</u> A(4MeTyr)PD <u>h</u> <u>C</u> ) V(Hyp)(4ClPhe)RP- CoNH <sub>2</sub> X = 3-methyl-6,7-dimethoxy- benzofuranoic acid	0.16 ± 0.02
135G4	[(4F,3ClPhOCH <sub>2</sub> CO)SAYPDSV(Hyp)(4ClPhe)RPG] <sub>2</sub> -K-CO <sub>2</sub> NH <sub>2</sub>	0.13 ± 0.01
135H12	[XLA(4MeTyr)PDA V(Hyp)(4ClPhe)RPG] <sub>2</sub> - K-CO <sub>2</sub> NH <sub>2</sub> 3X = 3-methyl-6,7-dimethoxy- benzofuranoic acid	0.15 ± 0.03, n = 6

<sup>a</sup>SE indicates duplicate measurements unless otherwise indicated. Hyp, L-*trans*-4-hydroxyproline; Aib,  $\alpha$ -aminoisobutyric acid; Dap, diamino propionic acid; 4 Pal, 4-pyridyl-L-alanine; Cha, 3-cyclohexyl-L-alanine; Nle, L-norleucine; hS, L-homo-serine; hC, L-homoCysteine; 3FABu, (2S)-2-amino-4,4,4-trifluorobutanoic acid; AspTtz, 2-amino-3-(2H-1,2,3,4-tetrazol-5-yl)propanoic acid.